Fluorine-Ion-Mediated Electrodeposition of Rhombus-Like ZnFOH Nanorod Arrays: An Intermediate Route to Novel ZnO Nanoarchitectures

Feng Xu,[†] Litao Sun,*[,†] Min Dai,[‡] and Yinong Lu[‡]

SEU-FEI Nano-Pico Center, Key Laboratory of MEMS of Ministry of Education, Southeast University, Nanjing 210096, People's Republic of China, and State Key Laboratory of Materials-Oriented Chemical Engineering, College of Materials Science and Engineering, Nanjing University of Technology, Nanjing 210009, People's Republic of China

Received: July 16, 2010; Revised Manuscript Received: August 6, 2010

Novel rhombus-like ZnO nanorod (NR) arrays were achieved via a facile two-step synthesis strategy based on first a low-temperature aqueous electrodeposition of vertically aligned rhombic ZnFOH NR arrays in the presence of fluoride and second a pyrolysis of ZnFOH intermediate into ZnO with the same morphology. The fluorine-ion-mediated electrodeposition mechanism of ZnFOH was confirmed for the first time, and the proposed formation process that the rhombus-like ZnO NRs characterized by mesoporous structure derived from the electrodeposited ZnFOH intermediate was corroborated by systematic structural characterization of the as-prepared products. A dye-sensitized solar cell (DSSC) based on the rhombus-like ZnO NR arrays with a larger surface roughness factor was assembled, and a higher conversion efficiency of 0.69% was attained in comparison to 0.47% of the DSSC based on the hexagon-like ZnO NR arrays electrodeposited in the absence of fluoride. Further, we demonstrate that the unique two-step synthesis strategy also possessed the capability of constructing complex nanoarchitectures with 1D rhombus-like ZnO NRs as the building blocks.

1. Introduction

In the past decade, growing interest has been focused on nanostructured semiconducting materials due to their fundamental scientific significance and potential technologic applications. Thereinto, zinc oxide (ZnO), an important semiconductor with a direct wide-band gap of ~3.37 eV and a high exciton binding energy of 60 meV at room temperature, has been one of the most popular issues in the domain of materials science, chemistry, physics, and nanotechnology. Espacially, ever since the first report of room-temperature ultraviolet lasing from ZnO nanowires,[1] substantial effort has been devoted to the fabrication of arrays of one-dimensional (1D) ZnO nanostructures due to their unique properties and astonishing applications in piezoelectric transducers,[2] optical waveguides,[3] field emissions,[4] chemical and gas sensors,[5] light-emitting diodes,[6] dye-sensitized solar cells (DSSCs),[7] and so forth. Therefore, various synthesis methods have been developed to construct 1D ZnO nanostructure arrays, such as chemical and physical vapor deposition,[8] electrodeposition,[9] metal−organic vapor phase epitaxy,[10] and solution-processed methods.[11] However, owing to the intrinsic crystal growth habit of the hexagonal wurtzite ZnO, most of the 1D ZnO arrays including nanowires, nanorods, and nanotubes exhibit a hexagonal cross-section along the axial direction. At most, some nanotips or nanoneedles can be formed by further epitaxial growth on the original hexagonal end planes.[12] Currently, it is still a challenge to easily alter the shape of 1D ZnO nanostructures with well-defined contour.

Besides the direct preparation methods commonly used for ZnO nanostructures, the indirect transformation from nanostructured ZnO precursors to ZnO nanostructures with the nearly same morphologies is another desirable option. In this respect, nanostructured ZnFOH is just a case in point and has been used as the intermediate to further produce ZnO nanostructures. For instance, Wu et al.[13] and Zhu et al.[14] have respectively reported the synthesis of 1D ZnFOH nanofibers and nanobelts through an ionic liquid ([Tmim][BF_4]) assisted microwave irradiation method. Further, Huang et al.[15] presented a hydrothermal route toward a nanowire network of ZnFOH, which was then converted into ZnO with the same morphology by calcination. However, their resultant ZnO products did not possess impressive well-defined shapes, and the employed methods also have difficulties in the attainment of a large-scale vertically aligned 1D array, which is crucial for the fabrication of nanodevices. In this regard, we have developed an entirely original two-step synthesis approach to achieving facilely large-scale arrays of ZnO nanorods (NRs) with unique rhombic cross sections along the axial direction.[16] The novel two-step strategy was composed of a general low-temperature aqueous electrodeposition of vertically aligned rhombus-like ZnFOH NR arrays and a solid-state crystal phase conversion from ZnFOH to ZnO, without altering the rhombic shape. So far, to the best of our knowledge, that is the first example for fabricating successfully rhombus-like ZnO NR arrays. However, the formation mechanism of ZnFOH NR arrays was not investigated in depth. Here, in this work, a fluorine-ion-mediated electrodeposition mechanism of ZnFOH was confirmed, and at the same time more systematic structural and component characterizations were performed to further corroborate the proposed formation process that the rhombus-like ZnO NRs characterized by mesoporous structures derived from the electrodeposited ZnFOH intermediate. Significantly, due to the requirement of the electrochemical process, good electrical contact between the rhombus-like ZnO NR arrays and the substrate has been achieved, and the size of the rhombus-like NRs could be well controlled only by tuning the electrochemical parameters. These advantages provide the rhombus-

* To whom correspondence should be addressed. Phone: +86-25-83792632, ext. 8813. Fax: +86-25-83792939. E-mail: slt@seu.edu.cn (L.S.).
[†] Southeast University.
[‡] Nanjing University of Technology.

10.1021/jp1066082
Published on Web 08/23/2010

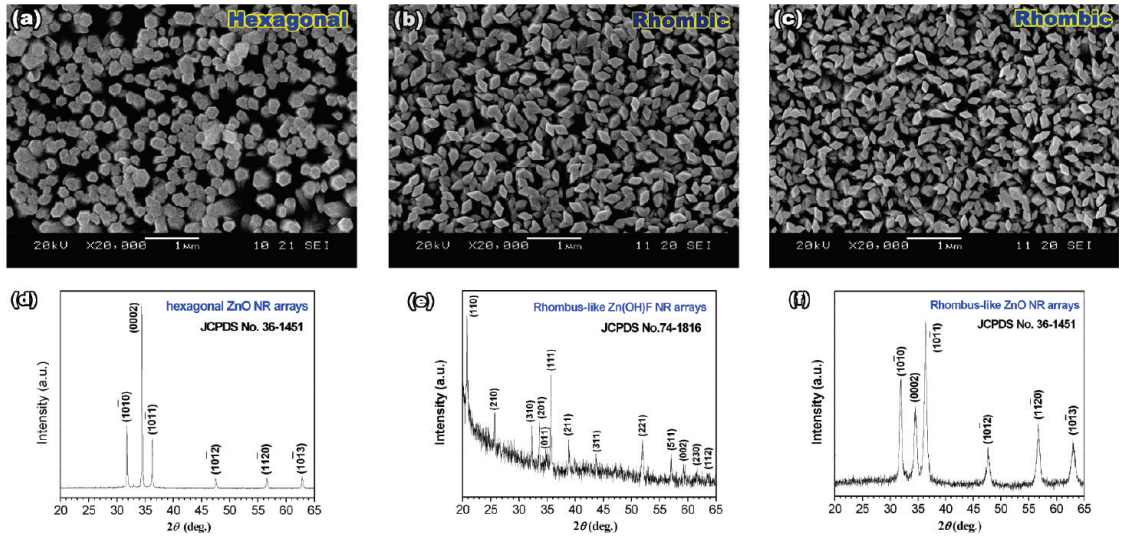

Figure 1. Top-view SEM images of arrays of (a) hexagonal ZnO NRs, (b) rhombic ZnFOH NRs, and (c) rhombic ZnO NRs. Parts d−f show the typical XRD patterns of the samples corresponding to parts a−c.

like ZnO NR arrays with great potential conveniences for applications in electronic and optoelectronic fields such as field emissions and dye-sensitized solar cells. We further demonstrated that the unique two-step synthesis strategy also possessed the capability of constructing complex nanoarchitectures with 1D rhombus-like ZnO NRs as the building blocks.

2. Experimental Section

All chemicals purchased from Shanghai Chemical Reagents Co. Ltd. are of analytical reagent grade and used as received without further purification. Typically, the electrodeposition of the rhombus-like ZnFOH NR arrays was potentiostatically performed in an aqueous electrolyte containing $Zn(NO_3)_2$ and NaF using a CHI660D electrochemical workstation (Shanghai Chenhua Instrument Co., China) with a classic three-electrode configuration that has been well documented.[17] Briefly, a piece of tin doped indium oxide (ITO, 10−15 Ω/□) glass substrate, a platinum plate, and a saturated calomel electrode (SCE) served as the working electrode (cathode), the counter electrode, and the reference electrode, respectively. The growth of ZnFOH NR arrays was assisted by spin-coating a thin film of ZnO nanocrystalline seeds onto ITO substrates.[18] Subsequently, the as-obtained ZnFOH sample was pyrolyzed at 450 □ for 2 h to yield unique rhombus-like ZnO NR arrays. Note that, since the rhombic ZnO NR arrays derived from the ZnFOH NR arrays, the size of the ZnO NRs is directly determined by that of the electrodeposited ZnFOH NRs which can be readily controlled by tuning the electrochemical parameters such as the electrolyte concentration and temperature, electrodeposition potential and duration, and the substrates.

The morphology and crystal phase identification of the products were investigated by scanning electron microscopy (SEM, JSM-5900, JEOL Ltd., Japan) and powder X-ray diffractometry (XRD, ARL XTRA, Thermo Electron Co., USA) with Cu Kα radiation, respectively. Further structural analysis of individual NR was carried out using transmission electron microscopy (TEM) and high-resolution TEM (HRTEM, JEM-2100, JEOL Ltd., Japan). The room-temperature photoluminescence (PL) spectra were recorded using a spectrophotometer (Jobin Yvon Fluorolog3-221) at an excitation wavelength of 325 nm. The fabrication procedure of dye-sensitized solar cells constructed using rhombus-like ZnO NR arrays is similar to our previous report.[19] The photocurrent−photovoltage ($I-V$) relationship of the cell was recorded under an AM 1.5G simulated sunlight (100 mW/cm^2) system with a CHI-660D electrochemical working station.

3. Results and Discussion

The electrodeposition of hexagonal ZnO NR arrays from an aqueous electrolyte only containing $Zn(NO_3)_2$ has been systematically investigated.[20] Figure 1a shows the typical surface topography of dense arrays of hexagonal ZnO NRs electrodeposited directly on the ZnO seedlayer/ITO substrate at −1.1 V for 0.5 h in 0.05 M $Zn(NO_3)_2$ aqueous solution kept at 50 □. The cross-section SEM image (see Figure S1 in the Supporting Information) reveals that these ZnO NRs of 150−200 nm in diameter are highly vertically aligned on the substrate and preferably oriented along the [0001] c-axis direction, as proved by the XRD pattern in Figure 1d. With adding 0.1 M NaF to 0.05 M $Zn(NO_3)_2$ aqueous solution and the other electrodeposition parameters being unchangeable, one can see that the whole substrate was successfully covered with the rhombic NR arrays (Figure 1b). These NRs with unique rhombus-like end planes are clear-cut in contour and radically different in shape from ZnO NRs with hexagonal end planes electrodeposited in the absence of NaF. The XRD pattern in Figure 1e corroborates the formation of rhombus-like ZnFOH NR arrays by this simple low-temperature aqueous electrodeposition, and all of the diffraction peaks can be indexed to the orthorhombic phase (SG: $Pna2_1$) with lattice constants $a = 10.13$ Å, $b = 4.760$ Å, and $c = 3.120$ Å, which is in good agreement with the literature values for orthorhombic-system ZnFOH (JCPDS 74-1816). No impurity peaks were detected, indicating the high purity of the as-prepared ZnFOH by the electrodeposition technique. In the previous reports on ZnFOH samples synthesized by solution-phase synthesis routes, no ordered 1D nanostructures were obtained. Herein, the electrochemical deposition facilely achieved the goal. Upon the subsequent pyrolysis of ZnFOH NR arrays, ZnO NR arrays with the same rhombic end planes were formed on the substrate, as shown in Figure 1c. By comparison, the rhombus-like shape of ZnO NRs remained unchanged, but the diameter seems to have become slightly smaller than that of ZnFOH NR arrays. The subtle difference in diameter should be related to the released component, HF, during the pyrolysis

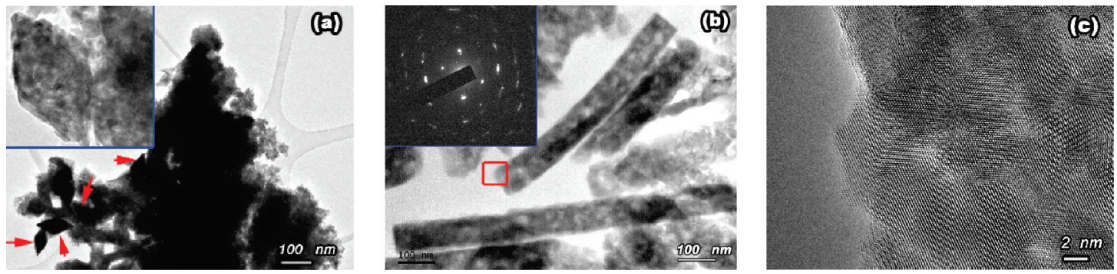

Figure 2. (a) Low-resolution TEM image of end planes (marked with the arrowheads) of rhombus-like ZnO NRs; the inset shows an individual rhombic end plane. (b) Low-resolution TEM image of side planes of rhombus-like ZnO NRs; the inset represents the SAED pattern on the side planes. (c) HRTEM image taken from the area marked with the frame in part b.

of ZnFOH according to eq 1. Figure 1f shows the typical XRD pattern of rhombus-like ZnO NR arrays with hexagonal wurtzite crystal structure (SG: $P6_3mc$, JCPDS 36-1451), confirming a crystal phase transformation from ZnFOH to ZnO upon a thermal treatment, without altering the original rhombic shape of ZnFOH NRs.

$$\mathrm{ZnFOH} \rightarrow \mathrm{ZnO} + \mathrm{HF}\uparrow \qquad (1)$$

To investigate further the crystal structure of the rhombus-like ZnO NRs, TEM and HRTEM images were observed, as shown in Figure 2. Figure 2a shows the low-resolution TEM image of end planes of rhombus-like ZnO NRs, proving clearly the presence of a rhombic shape corresponding to end planes (marked with the arrowheads). We find that a vigorous ultrasonic treatment for dispersing the samples before TEM observation did not damage the rhombic shape. An enlarged image on an individual rhombic end plane is inserted in Figure 2a to highlight the rhombic configuration that seems to be composed of nanoparticles and nanopores. Likewise, this structural characteristic was also observed on side planes of rhombus-like ZnO NRs, as shown in Figure 2b. The ring-like selected area electron diffraction (SAED) pattern (inset in Figure 2b) reveals the polycrystalline nature of the porous nanostructures. The subsequent HRTEM observation further gave the validation of the polycrystalline structure. The HRTEM image (Figure 2c) taken from the area marked with the frame in Figure 2b shows that no identical lattice fringes that generally reflect the crystal growth direction are clearly detected. Similarly, the as-electrodeposited ZnFOH NRs were also proved to be polycrystalline by the HRTEM observation (see Figure S2 in the Supporting Information). These HRTEM and XRD characterizations demonstrate that the polycrystalline nature of rhombus-like ZnO NRs should result from the polycrystalline precursor ZnFOH NRs, implying that both the polycrystalline structure and the rhombic morphology of the precursor are maintained, though a thorough solid-state crystal phase transformation from orthorhombic-system ZnFOH ($Pna2_1$) to hexagonal-system ZnO ($P6_3mc$) has occurred. It is worthwhile to note that the rhombus-like morphology of precursor ZnFOH NRs should be ascribed to the intrinsic crystalline habit of the orthorhombic-system crystals.

On the basis of the above-mentioned discussion, we consider that the synthesis of rhombus-like ZnFOH NR arrays is a prerequisite for the achievement of polycrystalline rhombus-like ZnO NR arrays. Therefore, further discussion should be mainly focused on the electrodeposition of the well-defined ZnFOH NR arrays. To date, to the best of our knowledge, the electrodeposition of ZnFOH crystals has not been achieved by other research groups, to say nothing of rhombus-like ZnFOH

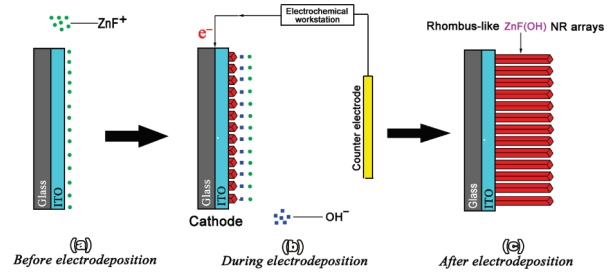

Figure 3. Schematic illustration of the electrodeposition process of the rhombus-like ZnFOH NR arrays on ITO glass substrates.

NR arrays. Herein, according to our understanding about chemical synthesis and the electrodeposition mechanism of ZnO that has been well documented,[20] a comparatively reasonable electrodeposition mechanism of ZnFOH is tentatively presented for the first time as follows. Before the electrodeposition, fluoride ions (F^-) and zinc ions (Zn^{2+}) coexist in the aqueous electrolyte and the two ions can form ZnF^+ complexes (eq 2)[21] that can freely diffuse to the surface of the conducting substrate, as shown in Figure 3a. During the electrodeposition, nitrate ions (NO_3^-) are reduced on the substrate by cathodic electrons provided by the electrochemical station, and a mass of hydroxyl ions (OH^-) are gradually generated (eq 3). Subsequently, with the help of these electrogenerated bases by reduction of NO_3^- ions, ZnF^+ ions and OH^- ions can easily combine into ZnFOH precipitate (eq 4) that can be firmly immobilized onto the substrate. This process is schematically illustrated in Figure 3b. Ultimately, after the electrodeposition, large-scale vertically aligned ZnFOH NR arrays can be formed according to the proposed formation mechanism corresponding to eqs 2−4, as shown in Figure 3c. Apparently, the preferential chemical combination between ZnF^+ complexes and electrogenerated OH^- ions prevented the formation of zinc hydroxide ($Zn(OH)_2$) via the combination of the free Zn^{2+} ions and OH^-ions that is characteristic in the electrodeposition mechanism of ZnO.[20] The existence of fluoride ions effectively interferes with the formation of ZnO. Thus, we designated the fluoride-ion-mediated formation process as fluoride-ion-mediated electrodeposition of ZnFOH.

$$\mathrm{Zn^{2+}} + \mathrm{F^-} \leftrightarrow \mathrm{ZnF^+} \qquad (2)$$

$$\mathrm{NO_3^-} + \mathrm{H_2O} + 2\mathrm{e^-} \rightarrow \mathrm{NO_2^-} + 2\mathrm{OH^-} \qquad (3)$$

$$\mathrm{ZnF^+} + \mathrm{OH^-} \leftrightarrow \mathrm{ZnFOH}\downarrow \qquad (4)$$

After having preliminarily understood about the electrodeposition mechanism of rhombus-like ZnFOH NR arrays, it is

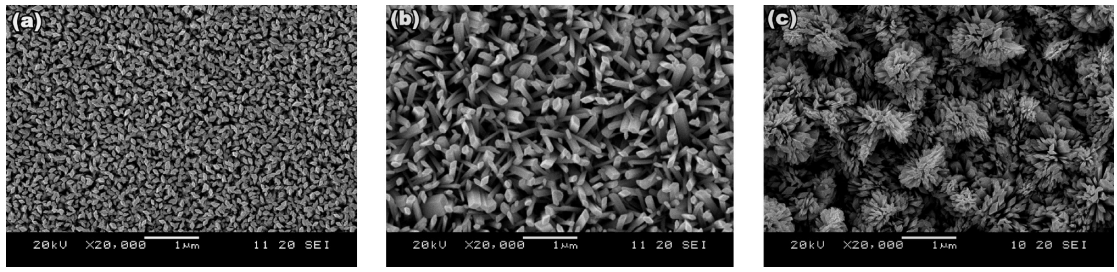

Figure 4. Top-view SEM images of arrays of rhombus-like ZnO NR arrays derived from rhombus-like ZnFOH NR arrays electrodeposited on ITO substrates with (a) a pre-electrodeposited ZnO seedlayer, (b) a preprepared ZnO seedlayer by dip-coating, and (c) a presputtered Au layer, respectively.

further expected that the morphology of ZnFOH NR arrays can be facilely controlled by tuning the electrochemical parameters such as the electrolyte concentration and temperature, the electrodeposition potential and time, and the substrates, which is just similar to the case of hexagonal ZnO NR arrays prepared by electrodeposition. Then, via a subsequent heat treatment of as-electrodeposited ZnFOH samples, the corresponding ZnO products with the same morphology can be obtained. For instance, using different seedlayer substrates can effectively tune the size, verticality, and density of rhombus-like NR arrays. Figure 4a shows that using a pre-electrodeposited ZnO seedlayer resulted in an obvious decrease in the diameter of the resultant rhombus-like ZnO NR arrays. In this case, the electrodeposition of the ZnO seedlayer was performed at −1.1 V for only 5 s from a 0.05 M $Zn(NO_3)_2$ aqueous electrolyte kept at a low temperature of 30 °C. Moreover, a sol−gel-derived ZnO seedlayer by dip-coating other than high-speed spin-coating technique greatly impaired the verticality of rhombus-like ZnO NR arrays (Figure 4b), which could be related to the distribution ununiformity of the nanocrystalline ZnO seedlayer fabricated by the dip-coating technique. Further, if an ITO substrate with a presputtered Au layer (see Figure S3 in the Supporting Information) was used, the density of rhombus-like ZnO NR arrays was increased and prolonging growth time even resulted in the formation of a highly dense NR cluster, as shown in Figure 4c. Here, this increase in the density of NR arrays is very similar to our early report on direct electrodeposition of ZnO films with single-crystalline petal-like architectures on the same Au/ITO substrate[22] and thus is still ascribed to the reduced interfacial tension and nucleation energy barrier due to the presence of the sputtered Au layer that result in an easier nucleation process, forming a large number of crystal nuclei for subsequent growth of dense rhombus-like NR arrays.

Our developed two-step synthesis strategy based on first the electrodeposition of vertically aligned rhombic ZnFOH NR arrays on conducting substrates and second the pyrolysis of a ZnFOH intermediate into ZnO with the same morphology not only can achieve 1D arrays of rhombus-like ZnO NRs but also possesses the capability of constructing complex nanoarchitectures composed of 1D rhombus-like ZnO NRs acting as the building blocks. It was demonstrated that 3D flower-like nanoarchitectures composed of many rhombus-like ZnO NRs (Figure 5a and b) could be readily obtained when the electrodeposition was performed at a low temperature of 30 °C and at −1.1 V in 0.05 M $Zn(NO_3)_2$ and 0.1 M NaF aqueous solution. Further, with other electrodeposition parameters being unchangeable, increasing the electrodeposition potential to −1.3 V resulted in the formation of 2D network-like nanoarchitectures that seem to be weaved by individual rhombus-like NRs, as displayed in Figure 5c and d. Apparently, the interlaced ZnO nanoarchitectures have hardly been fabricated by other synthesis

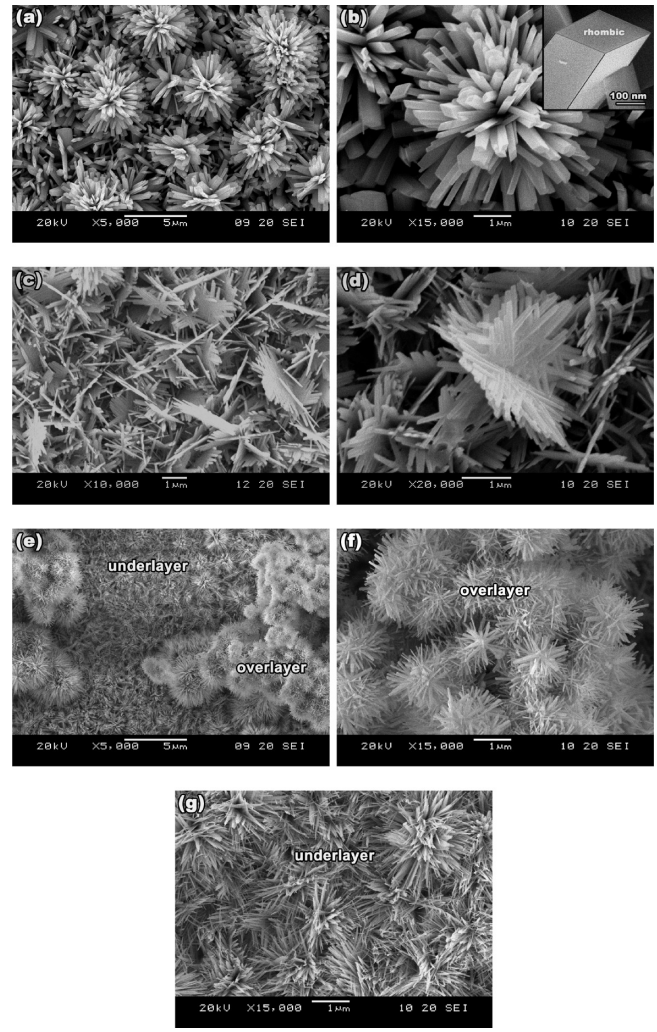

Figure 5. Various nanoarchitectures constructed by 1D rhombus-like ZnO NRs acting as the building blocks: (a, b) flower-like structures, (c, d) intertexture-like structures, and (e−g) double-layer structures obtained by a second electrodeposition route.

routes. If a two-step electrodeposition procedure was carried out in a diluted aqueous electrolyte (0.005 M $Zn(NO_3)_2$ and 0.01 M NaF), unusual double-layer nanostructures (Figure 5e) were also attained successfully, with the overlayer being dandelion-like nanostructures as the building blocks (Figure 5f) and the underlayer being the dense NRs with smaller diameter (Figure 5g). As to the formation mechanism of these complex nanoarchitectures obtained via the novel two-step synthesis strategy, a more in-depth investigation is still under way currently.

Crystalline ZnO NR arrays are good electrical conductors along the direction of the NR axes and thus are elegant for

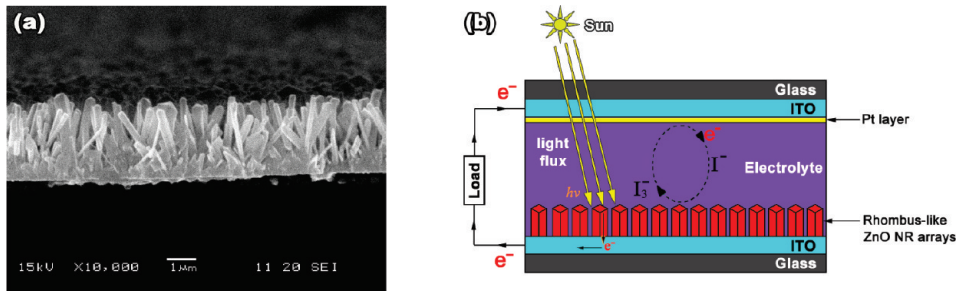

Figure 6. (a) Cross-section SEM image of rhombus-like ZnO NR arrays and (b) schematic diagram of the DSSC based on the rhombus-like ZnO NR arrays (note that, for clarity, the component of the photosensitizer is not shown here).

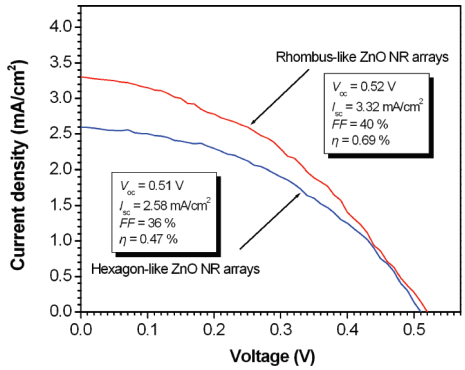

Figure 7. Current−voltage characteristic of the DSSC constructed using the hexagon-like ZnO NR arrays and the rhombus-like ZnO NR arrays, respectively, under a simulated illumination with a light intensity of 100 mW/cm^2 (AM 1.5).

applications in the fields of electronics and optoelectronics, especially dye-sensitized solar cells (DSSCs). The direct electrical pathways provided by the NR arrays ensure the rapid collection of photogenerated electrons throughout the photoanode of the DSSCs and thus avoid the trap-limited diffusion for electron transport encountered within the nanoparticulate photoanode films, a slow mechanism that can limit cell efficiency.[7] However, compared with the nanoparticulate photoanode films, insufficient internal surface areas intrinsically associated with the use of 1D NR arrays are unavoidable, which is adverse for loading more dye photosensitizer. In this regard, 1D ZnO nanostructured building blocks with a large surface area (characterized by a roughness factor[7]) are desirable in photoanodes of DSSCs. Here, polycrystalline rhombus-like ZnO NRs constructed by nanoparticles and nanopores should have larger surface areas than single-crystalline hexagonal ZnO NRs and thus are expected to further improve the DSSC efficiency. Therefore, the DSSC was assembled using an array film of rhombus-like ZnO NRs of ca. 200 nm in diameter and 3 μm in thickness (Figure 6a). The configuration of the DSSC based on the NR arrays resembles the schematic diagram illustrated in Figure 6b. At the same time, the control experiment was also performed using the DSSC constructed by single-crystalline hexagonal ZnO NR arrays prepared by direct electrodeposition in the absence of NaF that corresponds to the case of Figure 1a. For a more impartial comparison, the two types of ZnO NR arrays with nearly the same thickness (~3 μm) and diameter (200 nm) were selected to prepare the DSSCs.

Figure 7 shows the compared photocurrent−voltage ($I-V$) characteristics of both the DSSCs under a simulated illumination with a light intensity of 100 mW/cm^2 (AM 1.5). The short-circuit current density (I_{sc}), the open-circuit voltage (V_{oc}), the fill factor (FF), and the overall conversion efficiency (η) derived from the $I-V$ curves for both NR arrays based DSSCs are also inserted in Figure 7, respectively. It can be seen that the J_{sc} and FF values for the DSSC constructed using the polycrystalline rhombus-like ZnO NRs (J_{sc} = 3.32 mA/cm^2 and FF = 40%) show obvious improvement over the DSSC constructed using the single-crystalline hexagonal ZnO NRs (J_{sc} = 2.58 mA/cm^2 and FF = 36%). A higher J_{sc} would result in a higher η, since η is partly dependent on the J_{sc}.[23] Therefore, due to the much improved J_{sc} and FF, the rhombus-like ZnO NR arrays based DSSC attained a total power conversion efficiency of 0.69%, which is considerably superior to that of the hexagon-like ZnO NR arrays based DSSC (0.47%). By comparison, under the precondition of the nearly same sizes, the better photovoltaic performance of the rhombus-like ZnO NR arrays based DSSC should profit from more dye loading and light harvesting as a result of the enlargement of the internal surface area within the photoanode, which results from the rough surface characteristic of rhombus-like ZnO NRs constructed by nanoparticles and nanopores, as validated by TEM (Figure 2). Although nanopores existed among nanoparticles, the nanoparticles were not separated but tightly connected, which ensures the good electrical conduction among adjacent nanoparticles. Moreover, the evidence from room-temperature PL measurement also indicates the high crystalline quality of rhombus-like ZnO NR arrays, which is advantageous for rapid electron transferring. Figure S4 of the Supporting Information shows that, after the thermal treatment, ultraviolet (UV) emission of rhombus-like ZnO NRs shifted from 413 nm in the ZnFOH sample to 392 nm and visible emission related to intrinsic crystalline defects[24] was still kept at a low emission level. Therefore, it is deemed that the mesoporously structured rhombus-like ZnO NRs with high crystallinity can not only provide direct pathways for rapid electron transport but also increase the surface area for adsorbing more dye photosensitizer molecules to some extent.

4. Conclusions

In conclusion, novel rhombus-like ZnO NR arrays were successfully achieved by combining a general low-temperature electrodeposition route and a solid-state crystal phase transformation process. The synthesis of this new member in the family of 1D ZnO nanostructures could enrich our understanding about wurtzite crystal growth, and it presents a unique structural configuration with potential applications in electronic and optoelectronic fields. Dye-sensitized solar cells based on the polycrystalline rhombus-like ZnO NR arrays with about 200 nm in diameter and 3 μm in thickness attained an improved power conversion efficiency of 0.69% as compared to that based on the single-crystalline hexagon-like ZnO NR arrays. Moreover, the two-step synthesis method further demonstrates the capability of constructing complex nanoarchitectures composed of 1D rhombus-like ZnO NRs acting as the building blocks. This is an efficient and mild solution-based electrodeposition method

with clear advantages over the traditional high-temperature approach and also provides an elegant paradigm for developing the novel nanostructures of other functional materials.

Acknowledgment. We thank Prof. Zhonglin Wang from Georgia Institute of Technology for his help in studying the formation mechanism of rhombus-shaped ZnO nanorod arrays. This work was supported by the National Basic Research Program of China (No. 2009CB623702, No. 2011CB707601), the National Natural Science Foundation of China (No. 60976003, No. 51071044), China Postdoctoral Science Foundation Funded Project (No. 20100470066), Jiangsu Planned Projects for Postdoctoral Research Funds (No. 0902003B) and Open Research Fund of State Key Laboratory of Bioelectronics.

Supporting Information Available: Supplemental SEM, TEM, and PL data of ZnO and ZnFOH nanorods. This material is available free of charge via the Internet at http://pubs.acs.org.

References and Notes

(1) Huang, M. H.; Mao, S.; Feick, H.; Yan, H.; Wu, Y.; Kind, H.; Weber, E.; Russo, R.; Yang, P. D. *Science* **2001**, *292*, 1897.

(2) Tadashi, S.; Akira, K. *Appl. Phys. Lett.* **1974**, *25*, 10.

(3) (a) Jia, C. L.; Wang, K. M.; Wang, X. L.; Zhang, X. J.; Lu, F. *Opt. Express* **2005**, *13*, 5093. (b) Zhang, X. Y.; Hu, A.; Zhang, T.; Xue, X. J.; Wen, J. Z.; Duley, W. W. *Appl. Phys. Lett.* **2010**, *96*, 043109. (c) Johnson, J. C.; Yan, H. Q.; Yang, P. D.; Saykally, R. J. *J. Phys. Chem. B* **2003**, *107*, 8816.

(4) (a) Wei, A.; Sun, X. W.; Xu, C. X.; Dong, Z. L.; Yu, M. B.; Huang, W. *Appl. Phys. Lett.* **2006**, *88*, 213102. (b) Zeng, H. B.; Xu, X. J.; Bando, Y.; Gautam, U. K.; Zhai, T. Y.; Fang, X. S.; Liu, B. D.; Golberg, D. *Adv. Funct. Mater.* **2009**, *19*, 3165.

(5) (a) Hsueh, T. J.; Chen, Y. W.; Chang, S. J.; Wang, S. F.; Hsu, C. L.; Lin, Y. R.; Lin, T. S.; Chen, I. C. *Sens. Actuators, B* **2007**, *125*, 498. (b) Ahn, M. W.; Park, K. S.; Heo, J. H.; Kim, D. W.; Choi, K. J.; Park, J. G. *Sens. Actuators, B* **2009**, *138*, 168. (c) Law, J. B. K.; Thong, J. T. L. *Nanotechnology* **2008**, *19*, 205502.

(6) (a) Park, S. H.; Kim, S. H.; Han, S. W. *Nanotechnology* **2007**, *18*, 055608. (b) Zimmler, M. A.; Voss, T.; Ronning, C.; Capasso, F. *Appl. Phys. Lett.* **2009**, *94*, 241120. (c) Jeong, M. C.; Oh, B. Y.; Ham, M. H.; Lee, S. W.; Myoung, J. M. *Small* **2007**, *3*, 568.

(7) (a) Law, M.; Greene, L. E.; Johnson, J. C.; Saykally, R.; Yang, P. D. *Nat. Mater.* **2005**, *4*, 455. (b) Cheng, H. M.; Chiu, W. H.; Lee, C. H.; Tsai, S. Y.; Hsieh, W. F. *J. Phys. Chem. C* **2008**, *112*, 16359. (c) Lupan, O.; Guerin, V. M.; Tiginyanu, I. M.; Ursaki, V. V.; Chow, L.; Heinrich, H.; Pauporte, T. *J. Photochem. Photobiol., A* **2010**, *211*, 65. (d) Lee, Y. J.; Ruby, D. S.; Peters, D. W.; Mckenzie, B. B.; Hsu, J. W. P. *Nano Lett.* **2008**, *8*, 1501.

(8) (a) Wu, J. J.; Liu, S. C. *Adv. Mater.* **2002**, *14*, 215. (b) Lyu, S. C.; Zhang, Y.; Lee, C. J. *Chem. Mater.* **2003**, *15*, 3294.

(9) (a) Pauporte, T.; Bataille, G.; Joulaud, L.; Vermersch, F. J. *J. Phys. Chem. C* **2010**, *114*, 194. (b) Elias, J.; Tena-Zaera, R.; Levy-Clement, C. *J. Phys. Chem. C* **2008**, *112*, 5736. (c) Chang, M.; Cao, X. L.; Zeng, H. B. *J. Phys. Chem. C* **2009**, *113*, 15544.

(10) Park, W. I.; Kim, D. H.; Jung, S. W.; Yi, G. C. *Appl. Phys. Lett.* **2002**, *80*, 4232.

(11) (a) Xu, C. K.; Shin, P.; Cao, L. L.; Gao, D. *J. Phys. Chem. C* **2010**, *114*, 125. (b) Gao, Y. F.; Nagai, M.; Chang, T. C.; Shyue, J. J. *Cryst. Growth Des.* **2007**, *7*, 2467. (c) Martinson, A. B. F.; Mcgarrah, J. E.; Parpia, M. O. K.; Hupp, J. T. *Phys. Chem. Chem. Phys.* **2006**, *8*, 4655. (d) Qiu, J. J.; Li, X. M.; Zhuge, F. W.; Gan, X. Y.; Gao, X. D.; He, W. Z.; Park, S. J.; Kim, H. K.; Hwang, Y. H. *Nanotechnology* **2010**, *21*, 195602.

(12) Yang, Y. H.; Wang, B.; Xu, N. S.; Yang, G. W. *Appl. Phys. Lett.* **2006**, *89*, 043108.

(13) Wu, L. Y.; Lian, J. B.; Sun, G. X.; Kong, X. R.; Zheng, W. J. *Eur. J. Inorg. Chem.* **2009**, 2897.

(14) Zhu, L. J.; Zheng, Y. T.; Hao, T. Y.; Shi, X. X.; Chen, Y. T.; Ou-Yang, J. *Mater. Lett.* **2009**, *63*, 2405.

(15) Huang, Q. L.; Wang, M.; Zhong, H. X.; Chen, X. T.; Xue, Z. L.; You, X. Z. *Cryst. Growth Des.* **2008**, *8*, 1412.

(16) Xu, F.; Lu, Y. N.; Sun, L. T.; Zhi, L. J. *Chem. Commun.* **2010**, *46*, 3191.

(17) Xu, F.; Lu, Y. N.; Xie, Y.; Liu, Y. F. *Mater. Des.* **2009**, *30*, 1704.

(18) (a) Ohyama, M.; Kozuka, H.; Yoko, T. *Thin Solid Films* **1997**, *306*, 78. (b) Guo, M.; Diao, P.; Cai, S. M. *Appl. Surf. Sci.* **2005**, *249*, 71. (c) Baxter, J. B.; Walker, A. M.; Ommering, K. V.; Aydil, E. S. *Nanotechnology* **2006**, *17*, S304.

(19) Xu, F.; Dai, M.; Lu, Y. N.; Sun, L. T. *J. Phys. Chem. C* **2010**, *114*, 2776.

(20) Xu, F.; Lu, Y. N.; Xia, L. L.; Xie, Y.; Dai, M.; Liu, Y. F. *Mater. Res. Bul.* **2009**, *44*, 1700.

(21) Saito, N.; Haneda, H.; Seo, W. S.; Koumoto, K. *Langmiur* **2001**, *17*, 1461.

(22) Xu, F.; Lu, Y. N.; Xie, Y.; Liu, Y. F. *Vacuum* **2009**, *83*, 360.

(23) Chou, T. P.; Zhang, Q. F.; Fryxell, G. E.; Cao, G. Z. *Adv. Mater.* **2007**, *19*, 2588.

(24) (a) Khan, A.; Jadwisienczak, W. M.; Kordesch, M. *Physica E* **2006**, *33*, 331. (b) Zeng, H. B.; Cai, W. P.; Li, Y.; Hu, J. L.; Liu, P. S. *J. Phys. Chem. B* **2005**, *109*, 18260. (c) Vanheusden, K.; Seager, C. H.; Warren, W. L.; Tallant, D. R.; Voigt, J. A. *Appl. Phys. Lett.* **1996**, *68*, 403.

JP1066082